ACS Catalysis

pubs.acs.org/acscatalysis

Research Article

Adsorption and Reactivity of Chiral Modifiers in Heterogeneous Catalysis: 1-(1-Naphthyl)ethylamine on Pt Surfaces

Zihao Wang, Héctor Noé Fernández-Escamilla, Jonathan Guerrero-Sánchez, Noboru Takeuchi, and Francisco Zaera*

Cite This: *ACS Catal.* 2022, 12, 10514–10521

Read Online

ACCESS | Metrics & More | Article Recommendations | Supporting Information

ABSTRACT: The adsorption from solution onto a Pt surface of 1-(1-naphthyl)ethylamine (1-NEA), a chiral modifier used to introduce enantioselectivity in catalytic hydrogenation reactions, as well as its subsequent chemical reactivity, was characterized by a combination of kinetic catalytic measurements, surface-science experiments, and quantum mechanics calculations. By using both ^{1}H NMR and gas chromatography/mass spectrometry detection, it was determined that 1-NEA can undergo H-D exchange with D_2 in solution when promoted by supported heterogeneous Pt catalysts. *In situ* infrared absorption spectroscopy studies at the solid–liquid interface afforded the detection of vibrational features indicative of the formation of N–D bonds, and quantum mechanics calculations helped with the peak assignment and provided evidence supporting an H-D exchange mechanism involving the formation of an intermediate-adsorbed protonated 1-NEA species. The reaction proved to be general, as it was observed with r- and s-1-NEA, r- and s-2-NEA, and cinchonine, and on Pt/SiO_2 and Pt/Al_2O_3 catalysts. NEA adsorption and protonation through the amine N atom explain a number of reported but previously not fully understood observations and provide a way to envision the mechanism by which the NEA molecule bestows enantioselectivity to Pt hydrogenation catalysts.

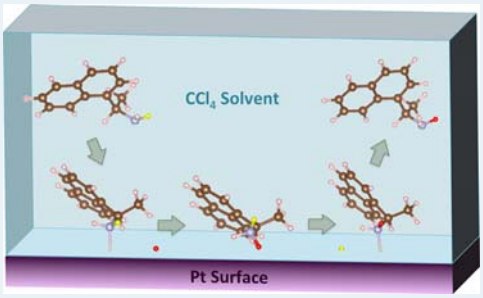

KEYWORDS: *enantioselectivity, chemisorption, protonation, catalysis, hydrogenation, surface modification, in situ infrared absorption spectroscopy, kinetics*

1. INTRODUCTION

It has been a long held dream to be able to design heterogeneous catalysts that exhibit the same level of selectivity as homogeneous counterparts.[1−3] Particularly challenging is to control chirality in catalytic processes associated with the manufacturing of pharmaceuticals, agroproducts, and other fine chemicals.[4−6] A promising route was introduced by Orito and co-workers, who showed that the addition of cinchona alkaloids to the reaction mixture during the hydrogenation of alpha-keto esters promoted by supported platinum catalysts renders the process highly enantioselective.[6,7] Unfortunately, our understanding of how these so-called chiral modifiers impart enantioselectivity to the metal catalysts is still limited, and the scope of the reactants for which this enantioselective hydrogenation catalysis can be used remains quite restricted. One key requirement for the molecular description of these systems is an understanding of the nature of the adsorption of the modifier.

On the basis of extensive surface-science studies using model metal surfaces and ultra-high vacuum (UHV) environments, it has been asserted that binding of both cinchona alkaloids and the simpler 1-(1-naphthyl)ethylamine (1-NEA) analog takes place primarily via their aromatic ring, which presumably lies flat on the solid surface.[8−10] Much of the early work by Baiker and co-workers, which included both experimental characterization of the adsorbed layers and quantum mechanics calculations, provided ample arguments for such bonding mode.[11−14] However, infrared absorption spectroscopy studies under more realistic conditions, which include the use of typical supported catalysts and the presence of a solvent (as these reactions are typically carried out in solution), have indicated that the orientation of the aromatic ring may depend on surface coverage, and that the adsorption geometry is central to defining the enantioselectivity of the catalytic process.[15−21] These systems have proven to be complex, with possible coadsorption of the chiral modifier in several configurations and arrangements, including modes where both the aromatic ring and the amine bind to the surface and where intermolecular interactions play a role in defining the geometry, especially at intermediate coverages.[22] Nevertheless, even in the more realistic cases, the adsorption of the chiral

Received: April 4, 2022
Revised: July 21, 2022

https://doi.org/10.1021/acscatal.2c01627
ACS Catal. 2022, 12, 10514–10521

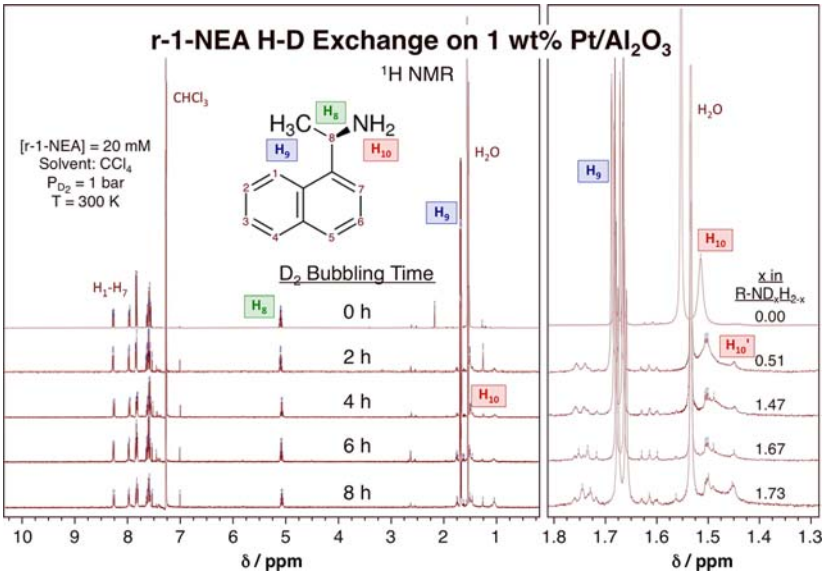

Figure 1. ^{1}H NMR of an r-1-NEA solution in CCl_4 as a function of the time it was exposed to an atmosphere of D_2 while in contact with a Pt/Al_2O_3 catalyst. Also provided are the structure of the r-1-NEA, with the corresponding carbon atom numbering, the peak assignment, and the average number of deuterium atoms incorporated in the amine group, estimated from the area of the peaks for H_{10} relative to those of the aromatic ring (spectra expanded on the right panel). The substitution of some amine hydrogens for deuteriums seen here provides clear evidence for a H-D exchange reaction and strongly suggests 1-NEA adsorption on the Pt surface via the amine N atom.

modifier has been assumed to take place mainly via the aromatic ring. On the other hand, recent work from our laboratory has suggested that perhaps bonding to the surface is dominated by the amine nitrogen atom instead.[23,24]

In the study reported here, we provide both spectroscopic and H-D exchange catalytic evidence that not only supports the model based on N-bonding adsorption of these amine-based chiral modifiers from solution but also indicates that the amine moiety is protonated on the surface. Results from complementary quantum mechanics calculations yielded additional evidence for such a model, and were used to estimate the energetics of the isotope exchange pathway observed experimentally.

2. EXPERIMENTAL DETAILS

The kinetic experiments on the H-D exchange reaction between 1-NEA (1-(1-naphthyl)ethylamine, either r- or s-, 99% purity, Sigma-Aldrich) and D_2 gas (Matheson, 99.5% atom purity) were carried out in an open glass flask. A set weight (25 mg) of a commercial 1 wt % Pt/Al_2O_3 catalyst (Alfa Aesar; Pt average nanoparticle size $\langle d \rangle = 3.4 \pm 0.1$ nm)[25] was added to a 20 mM NEA solution in CCl_4 (Sigma-Aldrich, 99.9%), and the mixture was then exposed to D_2 bubbled at atmospheric pressure while magnetically stirring. The reaction was run for 8.0 h, taking 1 mL aliquots for ^{1}H NMR or gas chromatography/mass spectrometry (GC−MS) analysis every 2.0 h. For the NMR tests, $CDCl_3$ (Millipore Sigma, 99.96% D, water <0.01%) was used for shimming and locking the magnetic field during NMR characterization, which was done using a Bruker Avance NEO 400 spectrometer. To avoid any possible H-D exchange between the NEA and the reference $CDCl_3$ solvent, the solution of the former was sealed in a capillary tube and placed inside the larger $CDCl_3$-containing NMR tube (more details, including the ^{1}H NMR spectra of the pure solvents, Figure S1, are provided in the Supporting Information). The GC−MS tests were carried out using the Agilent Technologies 5975 Series MSD apparatus.

The instrumentation used for the *in situ* attenuated total reflection infrared absorption spectroscopy (ATR-IR) characterization of the adsorbed species has been described in past publications.[24,25] Briefly, a Fourier transform infrared spectrometer (FTIR, Bruker Tensor 27) and a commercial multiple-bounce attenuated total reflection accessory (ATR, Pike Technologies) equipped with a 60 mm long Ge prism were used. A well-defined amount of the catalyst, typically 3 mg, was dispersed on the surface of the prism, and the ATR cell was filled with the pure solvent (CCl_4). The catalyst was preconditioned by bubbling either H_2 (Liquid Carbonic, 99.995% purity) or D_2 (Matheson, 99.5% atom purity) gas for 60 min, after which a background IR spectrum was taken. The cell was then exposed to a solution of the chiral modifier (NEA or cinchonine), and spectra were acquired every 30 min until surface saturation was reached. Afterward, the cell was flushed with the pure solvent, and additional spectra were recorded to differentiate between weakly and strongly bonded adsorbates. All the reported spectra were obtained by adding 256 scans taken with 4 cm^{-1} resolution and were ratioed against the reference spectrum recorded at the start of the experiment.

For the quantum-mechanics studies, spin-unrestricted first-principles calculations were performed based on periodic density functional theory (DFT) as implemented in the Vienna Ab initio simulation package (VASP)[26] with projector-augmented waves.[27] For the exchange-correlation (XC) potential, the generalized gradient approximation (GGA) with the Perdew−Burke−Ernzerhof (PBE) functional was employed.[28] Van der Waals interactions were considered using the Grimme D3 method.[29] The electronic states were expanded in plane waves with an energy cutoff of 400 eV. A c(8 × 4) surface unit cell was used, with four atomic layers and a 15 Å vacuum space added in the z direction, perpendicular to

https://doi.org/10.1021/acscatal.2c01627
ACS Catal. 2022, 12, 10514−10521

the surface. The bottom layer was fixed during the slab optimization and NEA adsorption. The Brillouin zone integration was done using a k-point grid of 7 × 7 × 1 within the c(8 × 4) cell. The geometric structures were optimized by minimizing the forces on individual atoms with the criterion that all forces on each atom must be smaller than 1×10^{-3} Ry/a.u. Vibrational frequencies were estimated by calculating the second derivative (Hessian matrix) of the potential energy surface using finite differences, and the corresponding intensities were derived from the dynamical dipole moments.[30] Two atomic layers were used, and atoms were displaced in all directions. The final frequencies were scaled[31−33] to optimize matching with the experimental values as indicated in the text. Reaction pathways and activation energies were calculated by using the nudged elastic band (NEB) method[34,35] within the climbing image scheme, as implemented in VASP. No reoptimization of the transition state structures was attempted as the simplicity of the reaction pathway, mainly involving the diffusion of hydrogen atoms on the surface, suggests that no major surface rearrangements are likely.

Although there are not many previous calculations on these systems that we can compare with (as they depend on the choice of van der Waals interactions), we found that our estimated adsorption energy for the most stable NEA flat geometry (E_{ads} = 3.94 eV, using Grimme D3) is close to that reported by Goubert et al. (E_{ads} = 3.54 eV, using optB88-vdW).[36] The effect of the solvent (CCl_4) was briefly evaluated by estimating the energy changes induced by coadsorbing CCl_4 with the flat configuration of NEA. It was found that the effect was minimal as the solvent only weakly physisorbs on the Cu surface.

3. RESULTS AND DISCUSSION

Initial evidence for the interaction of the amine nitrogen atom in the NEA molecule adsorbed from solution with platinum surfaces was obtained from reactivity studies using ^{1}H NMR and GC−MS analysis of NEA solutions as they were allowed to react with D_2 gas. Typical ^{1}H NMR data, in the case of r-1-NEA converted in the presence of a 1 wt % Pt/Al_2O_3 catalyst, are shown in Figure 1. The figure includes the corresponding peak assignment: the signals for the hydrogen atoms in the aromatic rings, H_1 to H_7, are detected at shifts above 7 ppm, whereas the hydrogen bonded to the alpha (chiral)-carbon of the ethyl moiety, H_8, appears at a shift slightly above 5 ppm. Particularly relevant to our studies are the hydrogen atoms in the terminal methyl group, H_9 (a doublet between 1.65 and 1.7 ppm), and those in the amine group, H_{10} (a broad feature around 1.5 ppm), which were seen to slowly exchange with deuterium. The growth of new peak, H_{10}', was also observed at approximately 1.45 ppm, which we assign to the remaining amine proton on the newly formed R-NHD H-D exchanged amine.

The substitution of H for D atoms in the amine group was quantified by using the areas of the H_{10} and H_{10}' peaks, scaled relative to the signal for six (H_1-H_6) of the protons of the aromatic ring (the signal for H_7 was excluded because it is a bit noisier); the resulting average number of D atoms incorporated in the reactant estimated using the H_{10} peak is provided in the right hand side of Figure 1. These data clearly indicate that the extent of the H-D exchange increases with reaction time. Slower and less extensive isotope exchange was also seen at the H_9 position (and possibly at the H_7 aromatic ring position), but the signal intensities of all the other hydrogen atoms remained approximately constant. The temporal evolution of the H-D exchange of all of the protons in the r-1-NEA upon exposure to D_2 in the presence of the Pt/Al_2O_3 catalyst is reported in Figure 2, in the form of the fraction of D

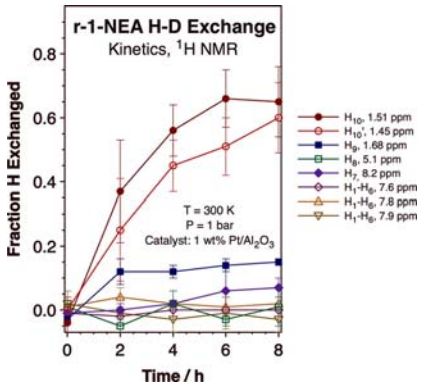

Figure 2. H-D exchange kinetics for r-1-NEA on Pt/Al_2O_3, measured using ^{1}H NMR. The values for the amine protons were calculated in two ways, using the intensities of the peaks at approximately 1.5 ppm (H_{10}) and 1.45 ppm (H_{10}'). The values and error bars were estimated using data from three independent kinetic runs.

incorporated at each position versus reaction time. Three independent kinetic experiments were carried out to estimate the error bars for these measurements (also shown in Figure 2), to make sure that the observed changes are not within the accuracy of the experiments (they are not). Data from a blank experiment, performed to corroborate that the changes observed are due to the Pt-promoted H-D exchange reaction, are reported in Section S2 of the Supporting Information. The kinetics estimated using the signals for the H_{10} and H_{10}' peaks agree with each other within our experimental error, a fact that provides additional confirmation of the Pt-catalyzed isotope substitution at the amine group of NEA.

Corroborating evidence for the H-D reaction with 1-NEA was provided by results from GC−MS experiments. An example of the resulting data is provided in Figure 3. The gas chromatograms displayed on the left panel show the growth of a small but sharp peak at a retention time of 7.60 min on top of the broad features due to the normal 1-NEA, a large peak between 7.45 and 7.6 min followed by a skewed trace extending to 8 min. The mass spectra reported in the right panel of Figure 3, obtained at 7.60 min, show not only the peaks expected for 1-NEA but also a growing feature at 172 amu, the mass of molecular 1-NEA-d_1. Quantitation of the growth of this peak is not viable as the new GC feature rides on top of a large background from regular 1-NEA, but what is clear is that the 172/171 amu ratio (172 and 171 amu being the values for the NEA-d_1 and NEA-d_0 molecular masses, respectively) does increase with reaction time (values provided in the right side of Figure 3). Both the ^{1}H NMR and the GC−MS data clearly prove that the H-D exchange of the hydrogen atoms in the amine group in 1-NEA with gas-phase D_2 is promoted by supported Pt catalysts (the blank experiments without the catalyst showed none of the changes seen in Figures 1 and 3; data provided in the Supporting Information). A small amount of decomposition of the NEA was also seen in these GC−MS experiments, as indicated by the growing peaks at 7.1 (1-naphthyl ethane) and 7.3 (1-naphthyl-1-D-methane) min in the GC traces (the corresponding MS data are provided

https://doi.org/10.1021/acscatal.2c01627
ACS Catal. 2022, 12, 10514−10521

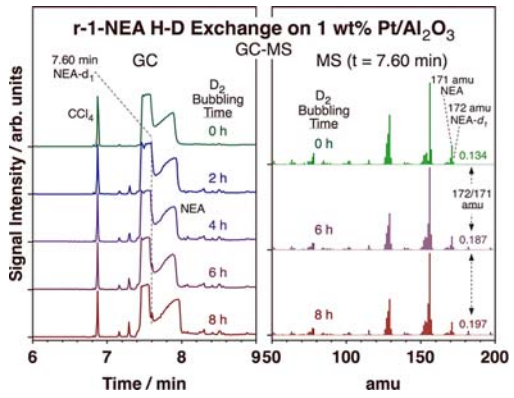

Figure 3. GC−MS data from experiments similar to those reported in Figure 1. The left panel displays the GC traces obtained for the reaction mixture as a function of time, which not only are dominated by the large peak at retention times between approximately 7.45 and 7.6 min but also show a skewed feature extending to 8 min and, crucially, a small but sharp new peak that develops over time at 7.60 min. The right panel, which shows the mass spectra of the mixture at 7.60 min elution time, highlights the presence of some deuterated 1-NEA, as indicated by the growth of the 172 amu peak.

in Figures S2 and S3, Supporting Information); these are minor and not relevant to the chemistry being discussed here.

The next question to address here is what the mechanism may be by which the H-D exchange occurs. Two straightforward and simple options can be put forward: the initial deprotonation of 1-NEA at the amine nitrogen upon adsorption followed by the addition of a deuterium atom from the metal surface, and the reverse deuteration of the amine position on the surface and the subsequent loss of a hydrogen atom. The energetics of these two possible reaction pathways was mapped out using DFT calculations; the results are shown in Figure 4 (red, top, traces for the first pathway; blue, bottom, data for the second). It is clear that, from the energy point of view, the second pathway, involving an initial protonation of the adsorbed NEA (blue trace), is favored as it requires overcoming a total energy barrier (to TS2, relative to the starting point) of only 76 kJ/mol; the first route, which involves an initial deprotonation step, displays an equivalent total barrier of 172 kJ/mol high (red trace). More details of these calculations, including drawings of the intermediate structures that form on the surface during the incorporation and ejection of H/D atoms into/from the adsorbed 1-NEA molecule, are provided in the Supporting Information.

The mechanism identified by these DFT calculations requires the formation of a protonated (deuterated) species at the amine group of 1-NEA on the Pt surface upon adsorption from liquid solutions. The molecular details of the adsorption of 1-NEA on the surface of the Pt catalyst that leads to the H-D exchange reaction were explored by using *in situ* ATR-IR. In these experiments, the catalyst is dispersed on the top surface of the prism of the ATR cell and exposed to a solution of 1-NEA (in CCl_4) while bubbling hydrogen or deuterium. It is interesting to point out that no detectable 1-NEA adsorption was ever seen without prior hydrogen bubbling, an observation consistent with the reported fact that these catalysts need to be preconditioned with hydrogen for the chiral catalysis to be operational.[37−39] In our case, a slow uptake of 1-NEA on the surface was observed over a period of 2−3 h, as already reported by us and others not only

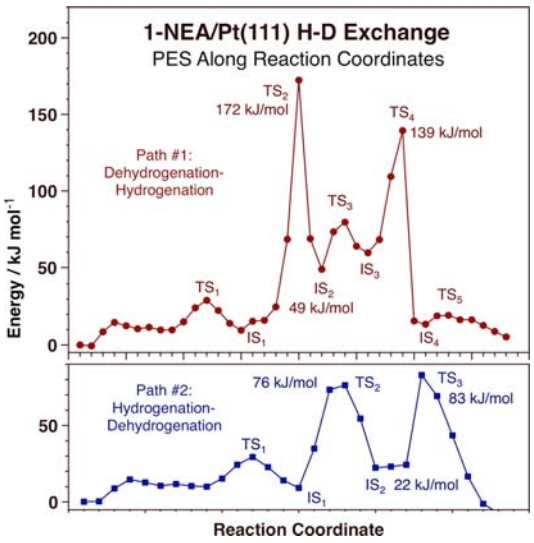

Figure 4. Calculated potential energy surfaces along the reaction coordinates for two possible mechanisms for the H-D exchange in 1-NEA promoted by Pt surfaces. In the top mechanism (red), the adsorbed NEA first loses an amine hydrogen atom and then adds a deuterium atom from the surface, whereas the bottom option follows the reverse sequence, namely, a surface deuterium atom is added first followed by the loss of an amine hydrogen. Clearly, the second mechanism is preferred in terms of the energy barriers that need to be surpassed.

with 1-NEA but also with cinchona alkaloids.[25,37,40] Figure 5 contrasts the 1-NEA uptake evolution when using H_2 versus

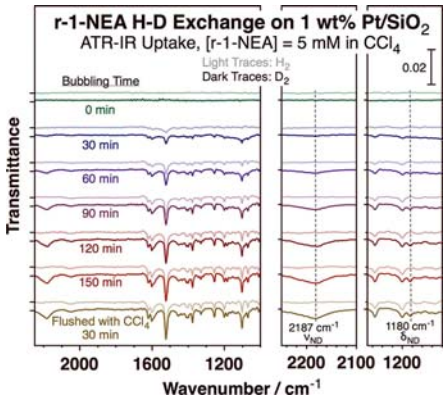

Figure 5. *In situ* ATR-IR spectra obtained during the uptake of r-1-NEA from a CCl_4 solution onto a Pt/SiO_2 catalyst while bubbling either H_2 (light traces) or D_2 (dark traces), plotted versus exposure time. Two new features grow in the case of D_2 bubbling not seen with H_2, around 1180 and 2187 cm^{-1}, as highlighted in the right two panels. These are indicative of the formation of N−D bonds. The system was flushed with a pure solvent (CCl_4) at the end of the run to corroborate that the adsorption is irreversible.

D_2. Pointedly, two new features are seen to grow in the spectra with D_2 not seen with H_2, at 1180 and 2187 cm^{-1} (the corresponding regions of the spectra are expanded in the two right panels of Figure 4). These signals, which are easily assigned to N−D deformation (δ_{ND}) and N−D stretching (ν_{ND}) vibrational modes, attest to the formation of new N−D bonds in the adsorbed 1-NEA.

https://doi.org/10.1021/acscatal.2c01627
ACS Catal. 2022, 12, 10514−10521

The behavior indicated in Figure 5 proved to be quite general. Figure 6, for instance, which displays the ATR-IR

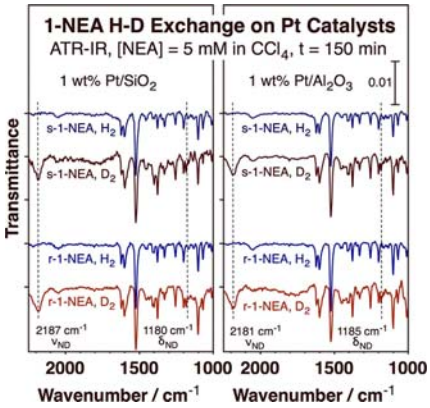

Figure 6. *In situ* ATR-IR spectra obtained after 150 min of uptake of either s- (top two traces) or r- (bottom two) 1-NEA from CCl_4 solutions onto a Pt/SiO_2 (left) or a Pt/Al_2O_3 (right) catalyst while bubbling either H_2 (blue traces) or D_2 (red traces). The deuterium incorporation in the N atom of 1-NEA when bubbling D_2 is indicated in all cases by the new features seen at 1180−1185 and 2181−2187 cm^{-1}.

spectra obtained at the end of the uptake of both r-1-NEA and s-1-NEA on either Pt/SiO_2 or Pt/Al_2O_3 catalysts, indicates the incorporation of deuterium into the 1-NEA molecule in all cases: the δ_{ND} (1180−1185 cm^{-1}) and ν_{ND} (2181−2187 cm^{-1}) peaks identified above are seen in all the spectra with D_2 but not in any of the experiments with H_2. The same behavior was seen with 2-NEA as well (Figure S4, Supporting Information). It should also be indicated that, under the conditions of these experiments, the NEA adsorption and the formation of the new surface intermediate (which we in this report argue is a protonated NEA) are irreversible, a conclusion indicated by the fact that flushing with a pure solvent after the uptake results in no changes in the positions or intensities of any of the IR peaks (bottom trace in Figure 5). No desorption is observed in any of these systems.

The ATR-IR data in Figures 5 and 6 clearly show the formation of a new N−D bond upon the bubbling of D_2 but that does not directly address the questions related to the structure of the adsorbed NEA. This is a particularly critical aspect of the study of enantioselective catalysis aided by chiral modifiers because the *in situ* IR spectra of the modifier adsorbed on the metal surface from liquid solutions have been shown to be very different from those acquired for the adsorbate in UHV or for the free molecules in solution.[41,42] It is clear that the presence of the liquid in contact with the catalyst affects the nature of the adsorbed molecules, but this effect cannot be fully ascribed to the solution alone. Complementary density functional theory (DFT) calculations were carried out to better understand these changes. First, the adsorption structures of pure 1-NEA and of NEA with one less or one more amine hydrogen (that is, deprotonated or protonated) were optimized, and simulated IR spectra were estimated to compare with the experimental data. The results are shown in Figure 7. The left panel reports the results, in the form of peak positions and peak intensities, for s-1-NEA in two different configurations, namely, adsorbed with the aromatic ring either flat or tilted with respect to the Pt surface, and for

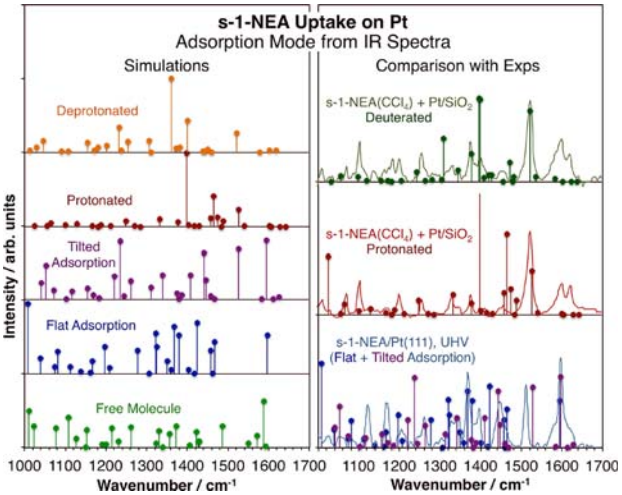

Figure 7. DFT-simulated IR spectra for s-1-NEA in different environments. Left: peak positions and peak intensities estimated from DFT calculations for (from bottom to top): the free molecule, the s-1-NEA adsorbed on Pt(111) with the ring either flat or tilted with respect to the surface plane, and the adsorbed molecule either protonated or deprotonated at the amine group. Right: best fits to the experimental spectra for s-1-NEA adsorbed on Pt(111) in UHV and on a Pt/SiO_2 catalyst from a CCl_4 solution. Also shown are the spectrum and best fit for the latter case when D_2 instead of H_2 is bubbled through the solution.

optimized adsorption geometries for the s-1-NEA molecule after either protonation or deprotonation of the amine group. It can be seen that all these options yield very different IR spectra. It should be noted, though, that the DFT IR simulations have a number of limitations and should therefore be analyzed with caution. For one, it is known that, because of the anharmonicity of the potentials around the minimum energy corresponding to the different bonds, quantum mechanics simulations miscalculate the true vibrational frequencies. This is typically addressed by scaling the frequencies in the calculated spectra using an empirical multiplicative factor;[31−33] that factor was optimized here to best fit the experimental data, as discussed later. In addition, the calculated peak intensities depend on adsorption geometries and do not account for the free rotation of the groups around single bonds that occurs within the ethylamine moiety in 1-NEA.

In spite of these shortcomings, we have here attempted to identify the nature of the adsorbed species using the simulated spectra. The key results are displayed in the right panel of Figure 7, and more details are provided in the Supporting Information (the vibrational peak assignments are slightly different from those provided in previous reports).[10,22,24,43] To decide on the simulated spectra that best interpret each of the experimental traces, a minimum square fitting of the frequency values (experimental minus calculated) was carried out with each option as a function of the scaling factor used in the calculations, and the results with the smallest standard deviation were chosen (the final scaling factors are tabulated in the Supporting Information). Three cases are shown in Figure 7. In the first case (bottom, light blue trace and blue and purple bars), the spectra for s-1-NEA adsorbed on Pt(111) under UHV are interpreted in terms of a combination of flat- and tilted-ring geometries; the best fit is to the tilted

https://doi.org/10.1021/acscatal.2c01627
ACS Catal. 2022, 12, 10514−10521

arrangement, but some important peaks are missed and only accounted for with a flat coadsorbate. It should be noted that most reports have concluded that NEA adsorption on bulk metal surfaces under vacuum leads to a flat geometry, as mentioned in the Introduction,[8,9] but a recent IR study has suggested the possibility of the formation of a tilted adsorbate at high coverages.[22]

The second comparison is for s-1-NEA adsorbed on a Pt/SiO_2 catalyst from a CCl_4 solution (red trace and bars), and it also applies to adsorption on either a Pt foil or a Pt/Al_2O_3 catalyst since those spectra all look similar (Figure 6 and previously published results).[24,42,43] In this case, the best fit is to a protonated NEA adsorbate, a result that not only is consistent with the H-D exchange reaction reported above but also helps explain a number of previously unaccounted for observations. First, the IR spectrum adsorbed from solution looks completely different from those obtained for the pure compound, for the compound dissolved in a liquid solvent, or for NEA adsorbed on Pt surfaces under vacuum.[41,42] It is possible that, while adsorption of NEA on the metal surface preserves the molecular stoichiometry of the chiral modifier, at a liquid−solid interface it leads to hydrogen incorporation, so the new IR spectra correspond to adsorbed protonated 1-NEA (1-NEA + H or 1-NEA + D) instead. We speculate that the solvent may help stabilize the additional charges added to the adsorbate after protonation; according to our Bader charge calculations, the electronic charge of the N atom goes from −0.89 in deprotonated 1-NEA (1-NEA-H) to −1.04 ± 0.02 in 1-NEA and to −1.13 in 1-NEA + H, all adsorbed on Pt(111) (Figure S5, Supporting Information).

The second observation explained by our data is the need for hydrogen pre-conditioning of the surface to induce the efficient uptake of chiral modifiers.[37−39] In fact, it has also been shown that the addition of acids to the solution to protonate the chiral modifier helps improve the enantioselective performance of the catalyst.[44] It should also be indicated that, in our *in situ* ATR-IR experiments, deuterium incorporation into the adsorbed 1-NEA is only seen if the surface is exposed to D_2 prior to the addition of the chiral modifier to the solution; bubbling of D_2 after 1-NEA surface saturation does not result in the development of the new IR peaks reported above (Figure S6, Supporting Information).

The third reported case in Figure 7 is that of s-1-NEA adsorbed from a CCl_4 solution while bubbling D_2 instead of H_2. Again, the fit of the DFT-calculated data to the experimental results is less than ideal, but the spectra are reasonably well accounted for by a monodeuterated adsorbed amine where the amine group rotates freely around its axis (the simulated spectrum in the figure is a weighted average of two extreme configurations, as shown in the Supporting Information). This amine protonation/deuteration seems to also be quite general: the development of the new N−D vibrational bands is seen not only in 2-NEA, as mentioned before (Figure S4, Supporting Information), but also in cinchonine (Cn), as shown in Figure 8. In this case, the two new features associated with the deformation (δ_{ND}^{+}) and stretching (ν_{ND}^{+}) modes of the N−D^+ bond that forms upon deuteration of the quinuclidine amine nitrogen are seen at 1210 and 1525 cm^{-1}, respectively. In addition, a new feature due to a ν_{NH}^{+} mode is seen at 2160 cm^{-1} in the spectrum for Cn adsorbed while bubbling H_2. Since quinuclidine is a tertiary amine, there are no N−H bonds in the free molecule, and no peaks for that vibration are seen in the spectrum for Cn dissolved in CCl_4

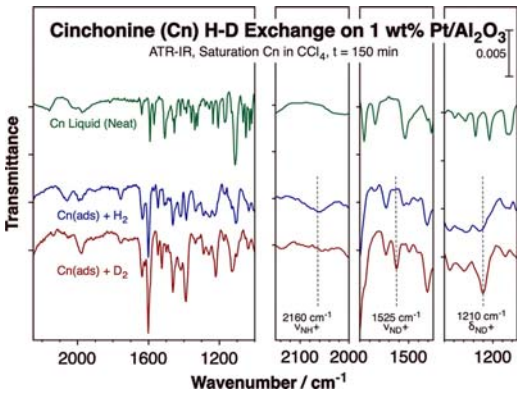

Figure 8. *In situ* ATR-IR spectra obtained after 150 min of uptake of cinchonine (Cn) from a CCl_4 solution onto a Pt/Al_2O_3 catalyst while bubbling either H_2 (middle, blue, trace) or D_2 (bottom, red, trace). The spectrum of Cn in solution (top, green) is also provided for reference. The deuterium incorporation to the N atom of the quinuclidine ring in Cn when bubbling D_2 is indicated by the new features seen at 1210 and 1525 cm^{-1} as well as by the disappearance on the peak at 2160 cm^{-1}.

(Figure 8, top, green, trace); only upon protonation of that amine it is possible to detect a N−H^+ stretching vibration. Notice also that the ν_{NH+} feature is not seen in the spectrum recorded while bubbling D_2 either. It is important to indicate that, although the values for the stretching frequencies reported here may appear low (typical values for N−H bonds are around 3500 cm^{-1}), this is because, in our case, the amine is protonated and has a positive charge; the reported frequency range for R≡N—H^+ stretching vibrations in dilute solutions is between 1800 and 2200 cm^{-1}.[45] Protonation of the amine (quinuclidine) nitrogen in cinchona alkaloid chiral modifiers upon adsorption on Pt in the presence of H_2 gas has in fact been proposed (but not proven) before.[46,47]

4. CONCLUSIONS

In this research, a combination of catalytic kinetic measurements, *in situ* infrared absorption spectroscopy characterization of adsorbed species, and quantum mechanics calculations was used to probe the surface chemistry associated with the adsorption and chemical reactivity of chiral modifiers, not only 1-NEA but also 2-NEA and cinchonine, at the liquid−solid interface of the type of Pt-based supported catalysis used to promote hydrogenation reactions enantioselectively. It was determined by using ^{1}H NMR and GC−MS detection that, in the presence of D_2 gas and a Pt catalyst, NEA undergoes H-D exchange at the amine nitrogen atom. DFT calculations indicated that the most likely mechanism for this reaction is via the formation of a protonated (deuterated) intermediate on the surface of the metal employed as a catalyst. *In situ* IR data were used to identify this species, which displays additional vibrational modes associated with the newly formed N−D bonds. These observations proved to be fairly general, as similar results were seen with both s and r enantiomers of 1-NEA and 2-NEA as well as with cinchonine and also with both Pt/SiO_2 and Pt/Al_2O_3 catalysts. The conclusion that NEA is protonated on the surface under reaction conditions, namely, in the presence of a solvent and as hydrogen is bubbled to the mixture, explains some observations not previously accounted for, including the unique nature of the IR spectra obtained for these adsorbed species when comparing with the free modifiers

https://doi.org/10.1021/acscatal.2c01627
ACS Catal. 2022, 12, 10514−10521

or for those adsorbed on Pt under vacuum, and also the need to precondition the surface with hydrogen for optimum adsorption and catalytic performance.

■ ASSOCIATED CONTENT

Supporting Information

The Supporting Information is available free of charge at https://pubs.acs.org/doi/10.1021/acscatal.2c01627.

^{1}H NMR of CCl_4 and $CDCl_3$ solvents, r-1-NEA + D_2(g) ^{1}H NMR H-D exchange reference (blank) experiment; MS of the minority GC peaks; DFT calculation of PES for the two most viable pathways for 1-NEA H-D exchange on Pt; *in situ* ATR-IR of 2-NEA on Pt catalysts, H_2 vs D_2 bubbling; IR spectra DFT simulations; DFT calculation of 1-NEA adsorption geometries on Pt(111), Bader c; *in situ* ATR-IR of 1-NEA, pre versus post D_2 conditioning of the Pt surface (PDF)

■ AUTHOR INFORMATION

Corresponding Author

Francisco Zaera − *Department of Chemistry and UCR Center for Catalysis, University of California, Riverside, California 92521, United States;* orcid.org/0000-0002-0128-7221; Email: zaera@ucr.edu

Authors

Zihao Wang − *Department of Chemistry and UCR Center for Catalysis, University of California, Riverside, California 92521, United States*

Héctor Noé Fernández-Escamilla − *Centro de Nanociencias y Nanotecnología, Universidad Nacional Autónoma de México, Ensenada, Baja California 22800, México*

Jonathan Guerrero-Sánchez − *Centro de Nanociencias y Nanotecnología, Universidad Nacional Autónoma de México, Ensenada, Baja California 22800, México;* orcid.org/0000-0003-1457-9677

Noboru Takeuchi − *Centro de Nanociencias y Nanotecnología, Universidad Nacional Autónoma de México, Ensenada, Baja California 22800, México*

Complete contact information is available at: https://pubs.acs.org/10.1021/acscatal.2c01627

Notes

The authors declare no competing financial interest.

■ ACKNOWLEDGMENTS

Financial support for this project was provided by a grant from the U.S. National Science Foundation, Division of Chemistry (NSF-CHE1854439). H.N.F.-E., J.G.-S., and N.T. thank DGAPA-UNAM projects IN105722 and IA100822 and Conacyt grant A1-S-9070 for partial financial support. The quantum mechanics calculations were performed in the DGCTIC-UNAM Supercomputing Center, funded by projects LANCAD-UNAM-DGTIC-051 and LANCAD-UNAM-DGTIC-368.

■ REFERENCES

(1) Zhang, L.; Zhou, M.; Wang, A.; Zhang, T. Selective Hydrogenation over Supported Metal Catalysts: From Nanoparticles to Single Atoms. *Chem. Rev.* **2020**, *120*, 683−733.

(2) Singh, B.; Sharma, V.; Gaikwad, R. P.; Fornasiero, P.; Zbořil, R.; Gawande, M. B. Single-Atom Catalysts: A Sustainable Pathway for the Advanced Catalytic Applications. *Small* **2021**, *17*, 2006473.

(3) Zaera, F. Designing Sites in Heterogeneous Catalysis: Are We Reaching Selectivities Competitive with Those of Homogeneous Catalysts? *Chem. Rev.* **2022**, *122*, 8594−8757.

(4) Blaser, H.-U. Chirality and Its Implications for the Pharmaceutical Industry. *Rendiconti Lincei* **2013**, *24*, 213−216.

(5) Zaera, F. Chirality in Adsorption on Solid Surfaces. *Chem. Soc. Rev.* **2017**, *46*, 7374−7398.

(6) Meemken, F.; Baiker, A. Recent Progress in Heterogeneous Asymmetric Hydrogenation of C═O and C═C Bonds on Supported Noble Metal Catalysts. *Chem. Rev.* **2017**, *117*, 11522−11569.

(7) Orito, Y.; Imai, S.; Niwa, S. Asymmetric Hydrogenation of a-Keto Esters Using a Platinum-Alumina Catalyst Modified with Cinchona Alkaloid. *J. Chem. Soc. Jpn.* **1980**, 670−672.

(8) Gellman, A. J.; Tysoe, W. T.; Zaera, F. Surface Chemistry for Enantioselective Catalysis. *Catal. Lett.* **2015**, *145*, 220−232.

(9) Dong, Y.; Goubert, G.; Groves, M. N.; Lemay, J.-C.; Hammer, B.; McBreen, P. H. Structure and Dynamics of Individual Diastereomeric Complexes on Platinum: Surface Studies Related to Heterogeneous Enantioselective Catalysis. *Acc. Chem. Res.* **2017**, *50*, 1163−1170.

(10) Zeng, Y.; Masini, F.; Rasmussen, A. M. H.; Groves, M. N.; Albert, V.; Boukouvalas, J.; McBreen, P. H. The Most Stable Adsorption Geometries of Two Chiral Modifiers on Pt(111). *Surf. Sci.* **2018**, *676*, 17−22.

(11) Schwalm, O.; Minder, B.; Weber, J.; Baiker, A. Enantioselective Hydrogenation of a-Keto Esters over Pt/Alumina Modified with Cinchonidine: Theoretical Investigation of the Substrate-Modifier Interaction. *Catal. Lett.* **1994**, *23*, 271−279.

(12) Baiker, A. Progress in Asymmetric Heterogeneous Catalysis: Design of Novel Chirally Modified Platinum Metal Catalysts. *J. Mol. Catal. A: Chem.* **1997**, *115*, 473−493.

(13) Diezi, S.; Mallat, T.; Szabo, A.; Baiker, A. Fine Tuning the "Chiral Sites" on Solid Enantioselective Catalysts. *J. Catal.* **2004**, *228*, 162−173.

(14) Baiker, A. Crucial Aspects in the Design of Chirally Modified Noble Metal Catalysts for Asymmetric Hydrogenation of Activated Ketones. *Chem. Soc. Rev.* **2015**, *44*, 7449−7464.

(15) Kubota, J.; Zaera, F. Adsorption Geometry of Modifiers as Key in Imparting Chirality to Platinum Catalysts. *J. Am. Chem. Soc.* **2001**, *123*, 11115−11116.

(16) Chu, W.; LeBlanc, R. J.; Williams, C. T.; Kubota, J.; Zaera, F. Vibrational Band Assignments for the Chiral Modifier Cinchonidine: Implications for Surface Studies. *J. Phys. Chem. B* **2003**, *107*, 14365−14373.

(17) Bartók, M.; Sutyinszki, M.; Balázsik, K.; Szöllodblacsi, G. Enantioselective Hydrogenation of Ethyl Pyruvate Catalysed by Cinchonine-Modified Pt/Al_2O_3: Tilted Adsorption Geometry of Cinchonine. *Catal. Lett.* **2005**, *100*, 161−167.

(18) Mink, L.; Ma, Z.; Olsen, R. A.; James, J. N.; Sholl, D. S.; Mueller, L. J.; Zaera, F. The Physico-Chemical Properties of Cinchona Alkaloids Responsible for Their Unique Performance in Chiral Catalysis. *Top. Catal.* **2008**, *48*, 120−127.

(19) Tan, S.; Williams, C. T. An In Situ Spectroscopic Study of Prochiral Reactant−Chiral Modifier Interactions on Palladium Catalyst: Case of Alkenoic Acid and Cinchonidine in Various Solvents. *J. Phys. Chem. C* **2013**, *117*, 18043−18052.

(20) Rodríguez-García, L.; Hungerbühler, K.; Baiker, A.; Meemken, F. The Critical Role of Tilted Cinchona Surface Species for Enantioselective Hydrogenation. *ACS Catal.* **2017**, *7*, 3799−3809.

(21) Jenkins, S. J. Chapter 7: Asymmetric Heterogeneous Catalysis. In *Chirality at Solid Surfaces*; John Wiley & Sons, Ltd.: online, 2018; pp. 225−255.

(22) Attia, S.; Spadafora, E. J.; Schmidt, M. C.; Schröder, C.; Baumann, A.-K.; Schauermann, S. Adsorption Geometry and Self-Assembling of Chiral Modifier (R)-(+)-1-(1-Naphthylethylamine) on Pt(111). *Phys. Chem. Chem. Phys.* **2020**, *22*, 15696−15706.

(23) Gordon, A. D.; Zaera, F. Adsorption of 1-(1-Naphthyl)-Ethylamine from Solution onto Platinum Surfaces: Implications for the Chiral Modification of Heterogeneous Catalysts. *Angew. Chem., Int. Ed.* **2013**, *52*, 3453−3456.
(24) Ni, Y.; Gordon, A. D.; Tanicala, F.; Zaera, F. Correlation between Chiral Modifier Adsorption and Enantioselectivity in Hydrogenation Catalysis. *Angew. Chem., Int. Ed.* **2017**, *56*, 7963−7966.
(25) Ni, Y.; Wang, Z.; Lee, I.; Zaera, F. Adsorption of Chiral Modifiers from Solution onto Supported Platinum Catalysts: The Effect of the Solvent, Other Coadsorbates, and the Support. *J. Phys. Chem. C* **2020**, *124*, 7903−7913.
(26) Kresse, G.; Furthmüller, J. Efficient Iterative Schemes for Ab Initio Total-Energy Calculations Using a Plane-Wave Basis Set. *Phys. Rev. B* **1996**, *54*, 11169−11186.
(27) Blöchl, P. E. Projector Augmented-Wave Method. *Phys. Rev. B* **1994**, *50*, 17953−17979.
(28) Perdew, J. P.; Burke, K.; Ernzerhof, M. Generalized Gradient Approximation Made Simple. *Phys. Rev. Lett.* **1996**, *77*, 3865−3868.
(29) Grimme, S.; Antony, J.; Ehrlich, S.; Krieg, H. A Consistent and Accurate Ab Initio Parametrization of Density Functional Dispersion Correction (DFT-D) for the 94 Elements H-Pu. *J. Chem. Phys.* **2010**, *132*, 154104.
(30) Baroni, S.; de Gironcoli, S.; Dal Corso, A.; Giannozzi, P. Phonons and Related Crystal Properties from Density-Functional Perturbation Theory. *Rev. Mod. Phys.* **2001**, *73*, 515−562.
(31) Alecu, I. M.; Zheng, J.; Zhao, Y.; Truhlar, D. G. Computational Thermochemistry: Scale Factor Databases and Scale Factors for Vibrational Frequencies Obtained from Electronic Model Chemistries. *J. Chem. Theory Comput.* **2010**, *6*, 2872−2887.
(32) Laury, M. L.; Carlson, M. J.; Wilson, A. K. Vibrational Frequency Scale Factors for Density Functional Theory and the Polarization Consistent Basis Sets. *J. Comput. Chem.* **2012**, *33*, 2380−2387.
(33) Kesharwani, M. K.; Brauer, B.; Martin, J. M. L. Frequency and Zero-Point Vibrational Energy Scale Factors for Double-Hybrid Density Functionals (and Other Selected Methods): Can Anharmonic Force Fields Be Avoided? *J. Phys. Chem. A* **2015**, *119*, 1701−1714.
(34) Henkelman, G.; Uberuaga, B. P.; Jónsson, H. A Climbing Image Nudged Elastic Band Method for Finding Saddle Points and Minimum Energy Paths. *J. Chem. Phys.* **2000**, *113*, 9901−9904.
(35) Henkelman, G.; Jónsson, H. Improved Tangent Estimate in the Nudged Elastic Band Method for Finding Minimum Energy Paths and Saddle Points. *J. Chem. Phys.* **2000**, *113*, 9978−9985.
(36) Goubert, G.; Rasmussen, A. M. H.; Dong, Y.; Groves, M. N.; McBreen, P. H.; Hammer, B. Walking-Like Diffusion of Two-Footed Asymmetric Aromatic Adsorbates on Pt(111). *Surf. Sci.* **2014**, *629*, 123−131.
(37) Ma, Z.; Kubota, J.; Zaera, F. The Influence of Dissolved Gases on the Adsorption of Cinchonidine from Solution onto a Platinum Surface: And in-Situ Infrared Spectroscopy Study. *J. Catal.* **2003**, *219*, 404−416.
(38) LeBlanc, R. J.; Chu, W.; Williams, C. T. Surface Raman Characterization of Cinchonidine-Modified Platinum in Ethanol: Effects of Liquid-Phase Concentration and Co-Adsorbed Hydrogen. *J. Mol. Catal. A: Chem.* **2004**, *212*, 277−289.
(39) Motobayashi, K.; Tomioka, R.; Uchida, T.; Osawa, M. Effect of Hydrogen on the Orientation of Cinchonidine Adsorbed on Platinum: An ATR-Seiras Study. *Chem. Lett.* **2015**, *44*, 770−772.
(40) Gordon, A. D.; Karakalos, S.; Zaera, F. Dependence of the Adsorption of Chiral Compounds on Their Enantiomeric Composition. *Surf. Sci.* **2014**, *629*, 3−10.
(41) Ma, Z.; Lee, I.; Zaera, F. Factors Controlling Adsorption Equilibria from Solution onto Solid Surfaces: The Uptake of Cinchona Alkaloids on Platinum Surfaces. *J. Am. Chem. Soc.* **2007**, *129*, 16083−16090.
(42) Zaera, F. Infrared Absorption Spectroscopy Characterization of Liquid−Solid Interfaces: The Case of Chiral Modification of Catalysts. *Surf. Sci.* **2018**, *669*, 16−24.
(43) Lee, I.; Ma, Z.; Kaneko, S.; Zaera, F. 1-(1-Naphthyl)Ethylamine Adsorption on Platinum Surfaces: On the Mechanism of Chiral Modification in Catalysis. *J. Am. Chem. Soc.* **2008**, *130*, 14597−14604.
(44) Blaser, H. U.; Jalett, H. P.; Wiehl, J. Enantioselective Hydrogenation of a-Keto Esters with Cinchona-Modified Platinum Catalysts: Effect of Acidic and Basic Solvents and Additives. *J. Mol. Catal.* **1991**, *68*, 215−222.
(45) Socrates, G. *Infrared Characteristic Group Frequencies: Tables and Charts*, 2nd ed.; Wiley: Chichester, 1994.
(46) Vargas, A.; Ferri, D.; Baiker, A. DFT and ATR-IR Insight into the Conformational Flexibility of Cinchonidine Adsorbed on Platinum: Proton Exchange with Metal. *J. Catal.* **2005**, *236*, 1−8.
(47) Olsen, R. A.; Borchardt, D.; Mink, L.; Agarwal, A.; Mueller, L. J.; Zaera, F. Effect of Protonation on the Conformation of Cinchonidine. *J. Am. Chem. Soc.* **2006**, *128*, 15594−15595.

https://doi.org/10.1021/acscatal.2c01627
ACS Catal. 2022, 12, 10514−10521